American Mineralogist, Volume 70, pages 288–303, 1985

Fluid inclusion geobarometry from ejected Mt. Somma-Vesuvius nodules

HARVEY E. BELKIN

U.S. Geological Survey
959 National Center, Reston, Virginia 22092

BENEDETTO DE VIVO

Centro di Studio per la Geocronologia e la Geochimica delle Formazioni Recenti
Istituto di Geochimica, Città Universitaria, Roma, Italy

EDWIN ROEDDER

U.S. Geological Survey
959 National Center, Reston, Virginia 22092

AND MASSIMO CORTINI

Istituto di Geologia e Geofisica
Largo San Marcellino 10, 80138 Napoli, Italy

Abstract

The Mt. Somma-Vesuvius volcano (Naples, Italy), part of the Italian-Tyrrhenian volcanic province, has erupted lavas and tephra that are silica-undersaturated and unusually potassium-rich. Ejected nodules, usually related to explosive activity, have been subdivided into four varieties: cumulate, "skarn," hornfels, and hypabyssal lava equivalents. The results of a microthermometric study of fluid inclusions from seven cumulate and three "skarn" nodules collected from the pyroclastics of three non-Plinian eruptive episodes are presented in this paper. Two primary inclusion types, formed by trapping of immiscible fluids, are commonly present: silicate melt (now glass in part crystallized to various daughter mineral(s) plus a shrinkage bubble) and essentially pure CO_2 (now liquid and vapor) $\pm$ glass. Three inclusions in one nodule (N81) contain water in addition to CO_2 and glass. The homogenization temperature (Th) of two-phase CO_2 inclusions was determined with a CHAIXMECA stage and used to derive the trapping density. In the seven cumulate nodules the CO_2 inclusion density ranged from 0.32 to 0.60 g/cm^3; those in the three "skarn" nodules ranged from 0.31 to 0.72 g/cm^3. Th of silicate melt inclusions, determined using a LEITZ 1350 stage, averaged $\sim$1200°C in cumulate and $\sim$1000°C in "skarn" nodules. CO_2 inclusion densities plus calculated P–V–T data on CO_2 at 1200° or 1000°C provide an estimate, with certain limitations, of the pressure during silicate melt and CO_2 inclusion trapping. These estimates range from $\sim$1200 to $\sim$3050 bars for seven cumulate nodules and from $\sim$925 to $\sim$3550 bars for the three "skarn" nodules. Assuming a density of 2.7 g/cm^3 for the magma column, the depth of trapping of both CO_2 and silicate melt inclusions was $\sim$4.5 to $\sim$11.0 km for the seven cumulate and $\sim$3.5 to $\sim$13.0 km for the three "skarn" nodules. Based on the presence of primary silicate-melt inclusions, both the cumulate and "skarn" nodules appear to have crystallized from a silicate melt. Two types of silicate-melt inclusions can be distinguished in the "skarn" nodules based on quenching behavior after homogenization; one quenches to glass, and the other readily crystallizes on quench. These two types suggest that melts of different composition were present in the "skarn" nodule environment. Cumulate and "skarn" nodules appear to be crystallization products from a silicate melt containing an emulsion of supercritical CO_2 globules. Most nodules contain CO_2 inclusions with a narrow density range but three nodules (N30, N13, N45) contain CO_2 inclusions that have an inexplicable bimodal distribution and wide density range.

0003–004X/85/0304–0288$02.00

Introduction

The Mt. Somma-Vesuvius region is noted for potassium-rich volcanic rocks and for the continuing controversy (cf. Varekamp, 1983 and Hermes and Cornell, 1983) over the relative roles of magmatic crystallization, mantle heterogeneity and various assimilation processes that produced nodules and distinctive petrological characteristics. Mt. Vesuvius is characterized by a dominant association of silica-undersaturated and potassium-rich rocks which were erupted during long periods of lava eruptions with only minor associated pyroclastic rocks. This sequence of small and intermediate scale eruptions was repeatedly interrupted by highly explosive Plinian eruptions (Santacroce, 1983). Volcanism in this region started at least 25,000 years ago and produced the Somma caldera which collapsed approximately 17,000 years ago (Delibrias et al., 1979). Vesuvius is the name given to the cone built up by the activity which followed the caldera collapse. The Somma activity was predominantly pyroclastic, whereas the Vesuvius activity after the 472 A.D. "Pollena" eruption has been predominantly effusive (Santacroce, 1983). The historical record for Vesuvius begins with the 79 A.D. Plinian eruption described by Pliny the Younger. Many varieties of nodules typically occur in abundance with the ejection of pumice and ash at the end of a non-Plinian eruptive episode; however, they are more or less common throughout the entire sequence.

We have examined ten nodules for fluid inclusions to attempt to deduce or place constraints on any physical parameters that might bear on nodule genesis. Mt. Vesuvius is located in a densely populated area. The volcano has been quiescent since April 1944 but because of its past volcanic history, it is potentially hazardous, especially during a Plinian eruptive phase (Bonasia et al., 1983). Thus, having a correct physical model of its behavior has scientific interest as well as important application in volcanic hazards assessment.

Geologic setting

Mt. Somma-Vesuvius system lies at the southern end of the so called "Roman Comagmatic" Province of Washington (1906) and north of the Calabrian arc (Gasparini et al., 1982). This region, lying just west of the Apennine Mts. along the Tyrrhenian Sea, is tectonically and petrologically complicated. A "peculiar" Benioff zone lying to the south of Vesuvius has been inferred by Gasparini et al. (1982), suggesting subduction of the continental lithosphere during the African and European continental collision. Ninkovich and Hays (1972) have interpreted the southern Italian volcanism, of which Vesuvius is a part, as an island-arc tectonic setting based on K_2O values that increase with increasing depth of origin as indicated by earthquake foci. However, the complete details of the local subsurface structure and tectonic history of the Somma-Vesuvius area are still somewhat obscure. Mt. Somma-Vesuvius lavas are K-rich and usually contain abundant phenocrysts of leucite and plagioclase. Mt. Somma lavas are phonolitic tephrites, whereas Mt. Vesuvius lavas are tephritic leucitites. Compositions transitional between these two types have not been observed (Savelli, 1967).

Other related potassium-rich volcanic areas are nearby. The Phlegraean Fields, located ~25 km west of Vesuvius, are a complex of eruptive centers that belong to the Quaternary potassium-rich rock series of the Roman province. The most recent eruption (Mt. Nuovo—1538 A.D.) was relatively small, but the eruption of the Campanian Ignimbrite ~35,000 years ago had an estimated volume of at least ~80 km^3 (Rosi et al., 1983).

Although the Mt. Somma-Vesuvius lavas have passed through many kilometers of carbonate rock that underlie Vesuvius, the relative contribution of carbonate and/or crustal assimilation to magma evolution is debated (cf. Rittmann, 1933 and Savelli 1968). Cortini and Hermes (1981), on the basis of the temporal variation of Sr isotopes, concluded that for Vesuvius, contamination was negligible. Turi and Taylor (1976) and Taylor et al., (1979) using oxygen isotopes concluded that there has been assimilation of shallow continental crust in the "Roman magmas" in the volcanic areas near and especially north of Rome but contamination of the lavas was minimal in the Vesuvius area. Hawkesworth and Vollmer (1979) also studied the question of crustal contamination versus enriched mantle and based on $^{143}Nd/^{144}Nd$ and $^{87}Sr/^{86}Sr$ argue for a recent mixing event in the upper mantle. The country rocks underlying the Mt. Somma-Vesuvius volcanic edifice are Mesozoic and Cenozoic carbonates of the Campanian-Lucanian carbonate platform (Ippolito et al., 1975), although the detailed stratigraphy and thicknesses are uncertain. Imbo (1950) estimated the sedimentary sequence beneath Vesuvius to be 5 to 6 km thick based on seismicity, and De Castro, as discussed in Savelli (1968), has estimated the combined thickness of three carbonate sequences (Triassic, Jurassic and Cretaceous) to be about 4500 to 5100 m. However, doubling of the carbonate sequences by faulting is common throughout the central-southern Apennines, and the possibility should be considered that the carbonates beneath Vesuvius are thickened by overthrusting (P. Scandone, pers. comm., 1982).

Analysis of the volcanic plumbing system beneath Mt. Somma-Vesuvius is of considerable importance for future eruption prediction and for the detailed study of previous eruptive history. Eruption dynamics differ between the Plinian eruptions and the common historical episodes of smaller-scale effusive activity. Barberi et al. (1981) and Sheridan et al. (1981) concluded that the two Plinian eruptions (79 A.D. and 3500 B.P.) they studied were fed by a magma chamber 2–4 km deep and ~2.0 km^3 in volume. However, Cortini and Scandone (1982), investigating Vesuvius eruptions between 1754 and 1944 (small or intermediate scale activity) concluded that mixing of magmas probably occurred in two deep-seated magma reservoirs (depth unspecified), each only ~0.1 km^3 in volume.

Previous studies of Mt. Somma-Vesuvius nodules

Nodules are abundant in the pyroclastics associated with Mt. Somma-Vesuvius lavas. The nodules are usually ejec-

ted during the later pyroclastic phases of an eruptive episode. Typical is the 1944 activity in which the ejection of scoriae, lava fragments and nodules marked a significant increase in presumably phreatic explosivity late in the eruption (Dolfi and Trigila, 1978). Similar nodules have been reported and studied from other nearby Italian volcanoes, such as Roccamonfina (Giannetti, 1982) and Vulsini (Varekamp, 1979). Nodules in Mt. Somma-Vesuvius ejecta were first described by Zambonini (1936) and have recently been studied intensively.

Hermes and Cornell (1978, 1981) have distinguished four varieties of nodule ejecta: (1) biotite-bearing pyroxenite, wehrlite, and dunite "accumulative" rocks, (2) metasomatized carbonates characterized by a recrystallized "skarn" assemblage, (3) recrystallized carbonate hornfels, and (4) shallow plutonic rocks (subeffusives). The "skarn" and "accumulative" rocks were studied in greater detail. From the lack of leucite they suggest that the "accumulative" (cumulate) rocks are a quenched, fractionated crystal mush that formed at "great" depths.

Hermes and Cornell (1981) have also analyzed the common interstitial glass in the cumulate nodules. They find the glass exhibits diverse compositions from sample to sample within the same eruptive episode and that this diversity encompasses the entire compositional range of the Vesuvian lavas and tephra. They proposed that the associated glasses represent diverse coexisting magmatic liquids extruded either from a zoned magma chamber or from independently evolved local pockets of magma separated from their common source. The "skarn" rocks were interpreted to represent highly metasomatized blocks of stoped basement carbonates incorporated into the magma. Carbonate xenolithic nodule ejecta have been studied by Savelli (1968) and by Barberi and Leoni (1980). Savelli (1968) concluded that Vesuvian carbonate ejecta indicated nonequilibrium assemblages with no direct evidence of assimilation but some evidence of metasomatic change by volcanic fluids and gases. Barberi and Leoni (1980) studied the carbonate ejecta in the Avellino pumice deposits (3500 B.P.) and the products of the 79 A.D. Plinian eruption. On the basis of the Mg content of calcite coexisting with dolomite they deduced an ejecta temperature range of 360 to 790°C and a fluid pressure not exceeding 1,500 to 2,000 bars, equivalent to a maximum depth of metamorphism of 5 to 6 km. Sorby (1858) studied the melt and aqueous inclusions in the minerals (idocrase, hornblende, calcite, nepheline, and feldspar) from the carbonate blocks ejected from Vesuvius and concluded that the minerals formed at 340 to 380°C and at a pressure equal to a depth of 1954 ft. (~0.6 km) to 3222 ft. (~1.0 km). Cundari (1982) studied clinopyroxenite nodules and their assemblages mainly from the "pyroclasts" emplaced during the 79 A.D. Plinian eruption. He also performed melting experiments and suggested a possible parental basanitic magma in the genesis of the leucite-bearing lavas.

Although the recent studies have advanced various plausible hypotheses for nodule origin there remain major unsolved problems at both Somma-Vesuvius and at Roccamonfina (Giannetti, 1982): (1) leucite phenocrysts are common in the Somma lavas and abundant in the Vesuvius lavas, but leucite is rare in cumulate nodules, (2) mica, which is abundant in many cumulate and "skarn" nodules is rare in the Somma-Vesuvius lavas, (3) it cannot be proven that the nodules and their host pyroclastics are cognate, and (4) there are problems regarding the depth, environment and conditions of nodule crystallization.

Another major reported occurrence of ejected plutonic nodules is from the Lesser Antilles island arc (Arculus and Wills, 1980). They describe similar problems of nodule origin, for example, in the Grenada lavas amphibole phenocrysts are rare but are abundant in the plutonic nodules.

Methods used

In addition to petrography we used crushing, heating and freezing stages for the study of fluid inclusions (Hollister and Crawford, 1981). Scanning of the slides at low magnification (~300×) was generally not effective because of the very small size of the inclusions. Most of the study required the use of a 100× oil-immersion objective. An ethyl chloride spray was used to cool seemingly empty inclusions in an attempt to condense a liquid phase. This was an important technique used to distinguish empty, decrepitated inclusions from CO_2 inclusions during the scanning of the slides. The crushing stage (Roedder, 1970) was used to verify the presence of high-pressure gases in the inclusions and to estimate their relative solubility in the crushing media. For homogenization of silicate-melt inclusions a LEITZ MODEL 1350[1] stage was used. It was calibrated at 1064.4°C by using pieces of pure gold (99.999%) similar to the mass of the sample. The precision of the stage was high (±10°C) but because calibration at the gold melting point indicated a 92°C stage correction, the accuracy was probably low. Different heating rates did not appreciably affect standardization but probably would affect silicate-melt inclusion homogenization, due to the sluggishness of silicate dissolution kinetics and diffusion.

For freezing and heating studies of the CO_2-rich inclusions, we used a CHAIXMECA stage (Poty et al., 1976) modified as described by Cunningham and Corollo (1980). The CHAIXMECA stage was used for two purposes. First, it was used to determine the triple point of previously frozen CO_2 inclusions (Tm–CO_2), which provides an estimate of the purity of the contents (pure CO_2 has a triple point of −56.6°C). Second, it was used to determine the homogenization temperature (Th) of the vapor and liquid CO_2 and the type of homogenization behavior. From such homogenization information, it is possible to estimate the bulk density of the inclusion fluid. The CO_2 inclusions are usually small and optically poor. Only inclusions large enough to be measured using a 32× long-working distance objective (e.g., LEITZ UTK-50 or L32) were used. Moving the adjustable substage condenser off axis was vital to resolve many of the CO_2 liquid–vapor menisci.

Near the vapor-liquid homogenization temperature, the rate of heating was approximately 0.1°C per five minutes. The precision of the stage was high (~±0.1°C) but the accuracy was difficult to assess in the specific homogenization temperature range of +28° to +31°C. Nevertheless, calibration standards, pure water and A. H. Thomas, Co. Micromelting standard *A* (+43.0°C), melt at their known temperature within the range of precision (±0.1°C).

[1] Any use of trade names in this report is for descriptive purposes only and does not constitute endorsement by the U.S. Geological Survey.

Table 1. Table showing nodule locality, eruption date, sample number, nodule type, SiO_2 content and modal composition.

Nodule Locality and eruption date	Sample no. and nodule type (Hermes and Cornell, 1978)	SiO_2* (wt.%)	Modal Composition* Pyroxene	Biotite	Apatite	Glass	Olivine	Opaque	Phlogopite	Spinel
Valle dell'Inferno = 1944 A.D.	N-1 cumulate	46.09	71.0	25.0	4.0	TR				
" " "	N-13 skarn	37.24	19.6						78.8	1.6
Villa Inglese = 1440-1631 A.D.	N-34 cumulate	N.G.	86.2	13.2	0.2	0.2	0.2			
" "	N-42 "	50.89	75.7	9.5		0.9	13.9	TR		
" "	N-45 "	N.G.	72.7	24.6	0.7		1.1	1.0		
" "	N-48 "	N.G.	80.4	17.9	1.4	0.3		TR		
" "	N-30 skarn	38.77	✓			✓	✓		✓	✓
Lagno di Pollena = <79 A.D.	N-62 cumulate	N.G.	59.8	38.8	4.5	0.9				
" " "	N-81 "	N.G.	92.3	4.5	3.2		TR			
" " "	N-67 skarn	38.10	1.4			0.3	12.0		74.2	12.1

*The modal composition and SiO_2 content were taken from Hermes and Cornell (1978). Our sections contain similar assemblages but perhaps not in their exact proportions (N-62 total equals 104% as given in Hermes and Cornell (1978)).

N.G. = not given, TR = trace, ✓ = phase present

Although the CHAIXMECA stage has an IR filter as an optical element it was necessary to place two additional IR filters in the light path to reduce the error in the homogenization temperature (especially near the critical point) from the absorption of IR by CO_2 in the inclusion. Using the procedures detailed above, we judge the homogenization temperature uncertainty to be in the range of ± 0.1°C.

In the range of $\sim -60°$ to -53°C the heating and cooling rates of our CHAIXMECA stage are difficult to control, hence the precision is low ($\sim \pm 1.0$°C). Although the stage theoretically can be precisely calibrated with the pure CO_2 inclusions supplied by the manufacturer, we judge the uncertainty of the CO_2 triple point (-56.6°C) to be approximately ± 1.0°C.

Samples studied

All our samples were from the suite studied and described by Hermes and Cornell (1978, 1981). Of the four nodule types they described, we investigated 7 cumulate and 3 "skarn" samples, as listed in Table 1. The nodules studied represent three separate eruptive episodes. One set of samples was collected from Valle dell'Inferno and represents material ejected in March 1944, during the last eruption of Vesuvius. The Villa Inglese samples were collected from a mudflow that underlies the 1631 A.D. lava and overlies the 1440 A.D. lava. Historical records (Alfano and Friedlander, 1929) suggest that mudflow activity preceded the outpouring of lavas during the 1631 eruption of Vesuvius, so the mudflow is assumed to be 1631 in age, rather than merely younger than 1440. The samples collected at Lagno di Pollena, on the NW flank of Mt. Somma, represent pre-79 A.D. activity. Modal compositions and SiO_2 content of the individual samples are given in Table 1; the sample numbers used are those of Hermes and Cornell (1978, 1981).

Multiple thick sections (40 to 500 μm) were cut from all nodules and doubly polished. This sample preparation is essential, since many of the inclusions found in the doubly polished plates would be lost during ordinary thin section preparation, and if not lost, would be more difficult to observe.

Description of nodules

Cumulate nodules. The seven cumulate nodules are clinopyroxenites with abundant biotite, minor apatite, glass and olivine. The nodules have common vugs or cavities that are filled or lined with glass and glass is also present between the individual grains. The texture is usually orthocumulate or heteradcumulate as defined by Wager et al. (1960). Orthocumulate texture in these nodules is characterized by visible zoning in euhedral to subhedral pyroxenes with intercumulus glass and mineral growth. In some thick sections, the pyroxenes and biotites have a pronounced preferred orientation. Micas also show common kinking or bending that appears to have occurred before solidification. The grain size is coarse ranging from 1 to 10 mm and the nodules are friable. Zoning is nearly ubiquitous in the pyroxenes. The heteradcumulates typically have 120° triple junction textures and lack obvious reaction phenomena.

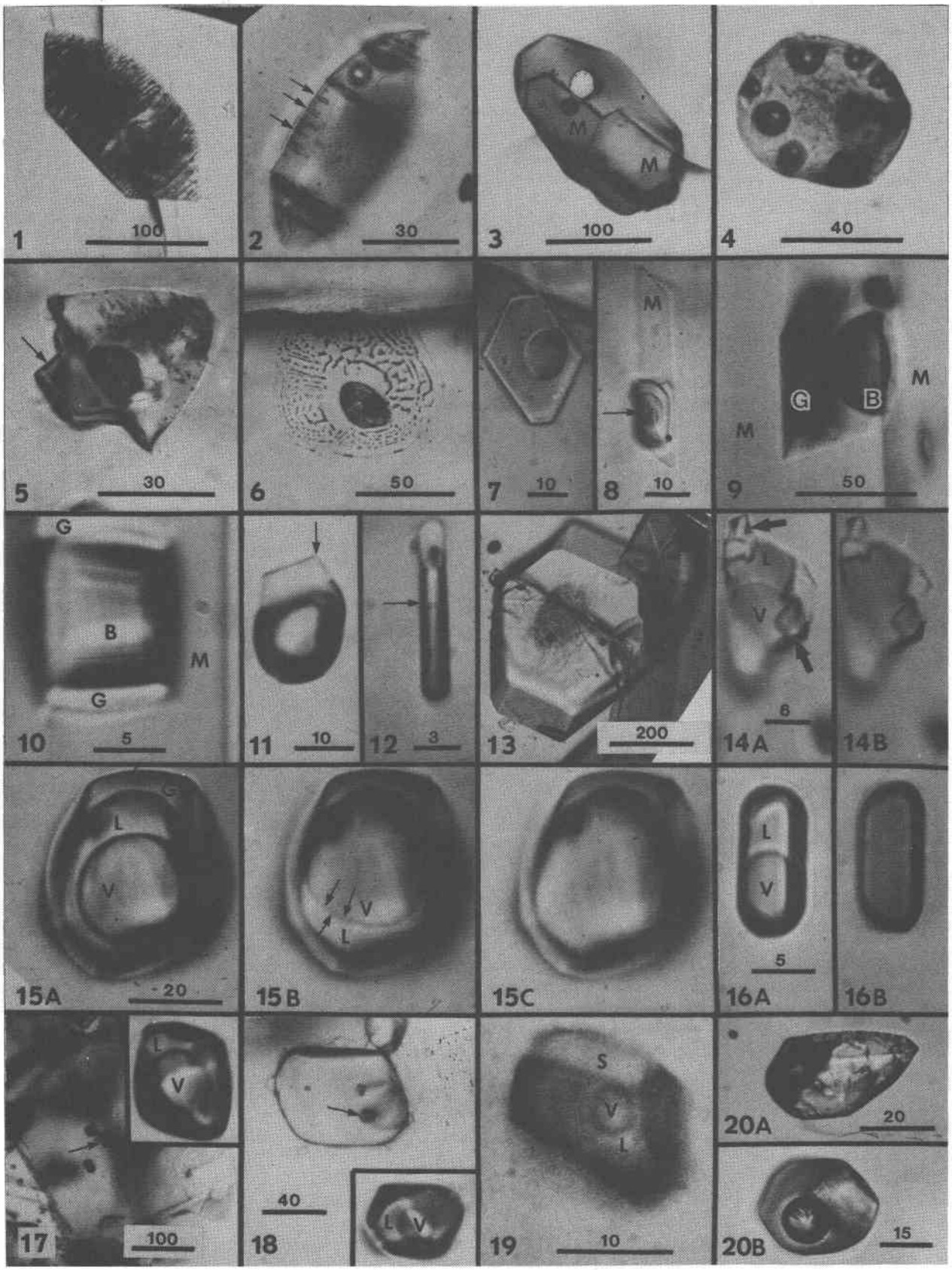
1
100
2
30
3
M
M
100
4
40
5
30
6
50
7
10
8
M
10
9
G
B
M
M
50
10
G
B
M
G
5
11
10
12
3
13
200
14A
V
6
14B
15A
G
L
V
20
15B
V
L
15C
16A
L
V
5
16B
17
L
V
100
18
40
L
V
19
S
V
L
10
20A
20
20B
15

All figures were photographed with plane-polarized transmitted light and all scale bars give measurements in micrometers.

Fig. 1. A typical primary silicate-melt inclusion in pyroxene from nodule N1. The inclusion has a negative-crystal shape and is similar to others in the same and nearby crystals. A large shrinkage bubble is near the center. Smaller bubbles are common, adhering to the epitaxial mica-daughter crystals. The bubbles did not contain any visible CO_2.

Fig. 2. A primary silicate melt inclusion in pyroxene from nodule N42. Numerous, small epitaxial mica-daughter crystals (arrows) can be seen along one side. Apparently these stopped growing before they transected the width of the inclusion.

Fig. 3. A primary silicate melt inclusion in pyroxene from nodule N48. Two hexagonal mica crystals (M) may or may not be daughter crystals.

Fig. 4. A primary silicate melt inclusion in pyroxene from nodule N81 with multiple bubbles set in partially devitrified glass. The optics were too poor to resolve any CO_2 in the bubbles, although a thin crack surrounds this inclusion, perhaps a result of decrepitation.

Fig. 5. A primary silicate-melt inclusion in pyroxene from nodule N34. A mica crystal (arrow) has adhered to the surface of a growing pyroxene crystal and caused melt to be trapped. A bubble preferentially wets the mica crystal.

Fig. 6. A primary silicate-melt inclusion in pyroxene from nodule N81 that has partially decrepitated, forming a characteristic circular halo around the inclusion. CO_2 was seen in this inclusion but the optics were very poor.

Fig. 7. A solid inclusion of mica that was trapped in pyroxene from nodule N42 with a globule of immiscible CO_2 fluid adhering to a (001) face. The CO_2 has subsequently leaked out, probably along the edge of the crystal, to a nearby crack. Similar silicate melt adhering to included micas is also common.

Fig. 8. A solid inclusion of mica (M) trapped in a pyroxene from nodule N62 that had an immiscible CO_2 fluid adhering to it during crystallization. This picture was taken at +23.2°C and the CO_2 vapor (arrow) is visible. The CO_2 vapor–liquid homogenized by expansion of the liquid phase at +30.2°C.

Fig. 9. A typical silicate-melt inclusion in mica (M) from nodule N62. The bubble (B), now empty, presumably contained CO_2 and preferentially wetted one of the mica (001) faces making up the inclusion walls. The silicate glass (G) has partially devitrified.

Fig. 10. A typical empty CO_2 inclusion in mica (M) from nodule N42. Most CO_2 inclusions trapped in mica also trapped silicate melt, now glass (G). The distribution of the glass was governed by the CO_2 bubble (B) preferentially wetting the (001) faces.

Fig. 11. A mica crystal (arrow) that by adhering to a growing surface of a pyroxene in nodule N34 caused a globule of immiscible CO_2 fluid to be trapped during subsequent pyroxene crystallization. The CO_2 homogenized in the vapor phase at +30.3°C. The photograph was taken at +23.2°C.

Fig. 12. A primary CO_2 inclusion in apatite from a crystal (Fig. 13) in nodule N1. This is a typical shape, elongated in the (0001) direction. The CO_2 vapor-liquid meniscus (arrow) is visible and the CO_2 phases homogenized in the vapor phase at +30.6°C.

Fig. 13. Euhedral apatite crystal projecting into a vug lined with silicate glass from nodule N1. Typical of apatites in the cumulate nodules is a core containing abundant primary silicate, solid, and CO_2 inclusions.

Fig. 14. A primary CO_2 inclusion in pyroxene from nodule N30. This inclusion trapped minerals (arrows) that appear not to be daughter crystals. 14A shows the inclusion at +23.2°C with liquid (L) CO_2 and vapor (V) CO_2. The CO_2 homogenized in the vapor phase at +30.2°C. 14B shows the inclusion at +32.0°C.

Fig. 15. A primary CO_2 inclusion in pyroxene from nodule N45. Fig. 15A shows the inclusion at +22.4°C with a well-defined meniscus separating vapor (V) CO_2 and liquid (L) CO_2. Silicate glass (G) is preferentially wetting the pyroxene surface. Fig. 15B shows the inclusion at +30.3°C near its homogenization point (+30.8°C in the vapor phase). The meniscus is very faint (arrows) and separates the two CO_2 phases vapor (V) and liquid (L). Fig. 15C shows the inclusion of +32.4°C.

Fig. 16. A primary CO_2 inclusion near the edge of a spinel crystal from nodule N30. Fig. 16A shows the inclusion at +23.2°C with liquid (L) and vapor (V) CO_2. 16B shows the inclusion at +32.7°C. The inclusion homogenized in the vapor phase at +30.4°C.

Fig. 17. A spinel crystal from a spinel band from nodule N30. The spinel crystal has three primary CO_2 inclusions near the center. The inset shows one CO_2 inclusion (arrow) at +23.2°C. The CO_2 inclusion has a typical negative crystal shape and vapor (V) and liquid (L) CO_2 can be seen. The CO_2 homogenized at +29.6°C in the liquid phase.

Fig. 18. A spinel crystal included in a pyroxene from nodule N13. The inset shows a CO_2 inclusion (arrow) at +23.5°C. The CO_2 inclusion has a typical negative crystal shape and the vapor (V) and liquid (L) CO_2 can be seen. The CO_2 homogenized at +29.6°C in the liquid phase.

Fig. 19. Primary dense CO_2 inclusion in the center of a spinel crystal from nodule N30. The CO_2 vapor (V) and liquid (L) phases at ~0.0°C can be seen with an unknown solid (S) phase. The bubble was moving at this temperature. This required fast film (3000 ASA) that decreased the resolution of the image. The CO_2 homogenized at +24°C in the liquid phase.

Fig. 20. (A) is an unheated primary silicate-melt inclusion in spinel from sample N30. This is typical of those that quench to a weakly birefringent crystalline material after homogenization. The irregularly shaped dark area on the left is the bubble. (B) is a primary silicate-melt inclusion in mica from sample N13. This type quenches to a clear glass after homogenization. The inclusion contains a weakly birefringent crystal, probably pyroxene (daughter crystal?) and the bubble is surrounded by a clear glass area.

"Skarn" nodules. The "skarn" nodules are mostly phlogopite, with spinel, olivine and fassaitic pyroxene. The spinel, analysed by Hermes and Cornell (1978) is an aluminous, Fe-poor hercynite with low Ti, Cr, Mn, and Ni contents. The nodules have many 120° mineral junctions and the individual mineral grains show no obvious evidence of reaction or zoning. The grain size is fine to medium grained (>0.5 to 2 mm). The nodules are somewhat friable but not to the same degree as the cumulate nodules. Sample N30 has euhedral to subhedral spinels in bands, and sample N67 shows a strong preferred orientation of the micas.

Description of inclusions

Most of the fluid inclusions found represent the trapping of two immiscible fluids, silicate melt and supercritical CO_2 fluid. These two fluids were trapped, in various ratios, in individual inclusions that are mostly primary in origin. The silicate-melt inclusions were found in all the phases of all the nodules. CO_2 inclusions were also found in all samples but were less numerous. Water was found as a minor phase in three CO_2 inclusions in nodule N81.

Silicate-melt inclusions. Primary, secondary, and perhaps pseudosecondary inclusions occur in all nodules, both cumulate and "skarn." Secondary inclusions are very common in "skarn" nodules, but are rare in cumulate nodules. We have studied only primary silicate-melt inclusions that represent the trapping of silicate melt that was presumably in (local) equilibrium with the host crystal. They now consist of silicate glass, or its devitrified equivalent, randomly trapped mineral phases, daughter crystals, plus a shrinkage bubble, which may be single (Fig. 1, 2, 5) or multiple (Fig. 4). Use of the crushing stage reveals that most of the inclusion bubbles are essentially vacuum as they fill instantly when crushed in oil at room pressure. However, some of the bubbles appear to be too large to be formed by shrinkage alone, given the temperature of trapping and the small difference between the coefficients of expansion of silicate melt and crystal host. On crushing, these too-large bubbles reveal that they contain gas (presumably CO_2) under pressure. Two phases (liquid plus vapor) could be seen in a few of these bubbles but the optical images were too poor to determine *T*h.

One or more crystals are present in most of the inclusions; these may have precipitated from the melt after entrapment (i.e., they are daughter crystals, Fig. 2) or may have been crystals accidentally trapped along with the melt during the inclusion formation (Fig. 5). This distinction may be very difficult to resolve, especially in these Mt Somma-Vesuvius nodules. Critical to the analysis is knowledge of the trapped melt composition. The cumulate nodules contain abundant cumulate phases that are rare in the lavas. For example in Fig. 3 (nodule N48) two large adjacent mica crystals comprise about 15 volume percent of the inclusion—glass and the bubble represent the balance. Lavas erupted from Vesuvius during the interval 1440 to 1631 A.D. contain less than 2 volume percent biotite (Savelli, 1967) but the biotite content of N48 is 17.9 volume percent (Hermes and Cornell, 1978). If the high biotite content of the nodule represents a biotite concentration process from a relatively biotite-poor magma, then one may conclude that the two mica crystals are not daughter crystals but have been accidentally trapped. However, if the nodule is a crystallization product from a contaminated or hybrid melt, then the two mica crystals could be daughter crystals. A dark opaque globule, possibly immiscible sulfide(?) was sometimes observed but not analyzed.

The primary silicate-melt inclusions range in number from a few to >100 in each crystal; their diameter ranges from a few μm to >200 μm. Although not always the case, the smaller ($\sim$10 μm) silicate-melt inclusions tend to consist of only glass plus shrinkage bubble and the larger ones tend to contain crystals as well. Some tend to have negative crystal shape, whereas others of similar size in the same nodule do not.

CO_2 inclusions. Primary CO_2 inclusions occur in all the transparent mineral phases (see below for discussion of mica). Apparently, the CO_2 was always trapped (Fig. 15) along with a small amount of melt (now glass and sometimes almost invisible). This glass (sometimes devitrified) occurs along the inside surface of the inclusions, preferentially in the areas of greatest curvature. Glass thickness and amount vary, $\sim$1 to $\sim$10 volume percent, and seem to be unrelated to the overall inclusion size.

Some CO_2 inclusions (Fig. 11) appear to have been trapped as a result of CO_2 globules adhering to various grains attached to the growing surface of the host crystal. These are primary inclusions (Roedder, 1976, Table III). Most other CO_2 inclusions also appear to be primary; they are isolated, relatively large with respect to the host and some (in spinels) outline growth of the host. Some are negative crystals, others are not. They range in diameter from $\sim$4 to $\sim$90 μm. Rare CO_2 inclusions that occur along healed fractures are thought to be secondary although they may be pseudosecondary in some cases. Occasionally CO_2 inclusions trapped mineral grains (Fig. 14) that appear not to be daughter crystals. Necking down was rarely observed. Secondary inclusions are more common in apatite and olivine than in spinel and pyroxene.

The abundance of the CO_2 inclusions in individual crystals, different minerals and different nodules varied widely. Most striking was the variability from grain to grain in the same sample. A few crystals in a thick section contained many CO_2 inclusions while many hundreds of others surrounding it had none. The estimated amount of CO_2 in the thick sections ranged from a few parts per billion to a few parts per thousand. Most thick sections contained a few parts per million of CO_2. The number of CO_2 inclusions measured does not represent the relative distribution of CO_2 inclusions in the nodules, but only those large enough and sufficiently clear to measure.

Several tests were carried out to verify the CO_2 composition (Roedder, 1965), including the crushing stage, thermal expansion, critical phenomena and infrared absorption. Although CO_2 inclusions are common in some of these samples, they are optically poor (especially affecting

the resolution of the vapor-liquid meniscus) and hence only a limited number permitted precise observations of the phase transitions.

The CO_2 inclusions in some spinels (in the "skarn" nodules) have a unique and enigmatic distribution. In the centers of the spinels, the inclusions are more numerous, have a greater CO_2 density (Fig. 19), and generally have a negative crystal shape (Fig. 17). However, in the outside portions of the same spinels, the CO_2 inclusions are less numerous, have a lower CO_2 density and usually do not have negative crystal shape. Other crystals have relatively low density CO_2 inclusions along the edges but no dense central CO_2 inclusions and vice versa. The density range of the CO_2 inclusions in the spinels from the same thick section is nearly as great as the density range for all the nodules. Spinels are common as solid inclusions in pyroxene and mica and, some of these included spinels have CO_2 inclusions (Fig. 18).

Primary CO_2 inclusions in apatite (Fig. 13) usually have a tubular shape (Fig. 12), arrayed parallel to the c-axis of the host and are in the cores of the grains. Apatites are common as solid inclusions in pyroxenes and micas and frequently these included apatites will have CO_2 inclusions.

We found no intact CO_2 inclusions in the micas, although numerous inclusions (Fig. 9 and Fig. 10) were found that probably represent trapped CO_2 that has since leaked (decrepitated). These usually appear to be negative crystals, hexagonal in outline and flattened parallel to (001) of the mica.

Decrepitated CO_2 inclusions. Inclusions of dense CO_2 fluid were trapped at depth; on ascent through the volcano conduit, the external pressure decreased, but the internal pressure in the inclusion remained essentially unchanged. Apparently some minerals in some nodules did not have enough strength to sustain the pressure differential during ascent, and hence show evidence of natural decrepitation and complete or partial loss of gas. This was recognized in all samples, but was not common, except in all the micas and the pyroxenes in nodule N1. Decrepitated inclusions sometimes show a characteristic aureole (Fig. 6). In this example, the fracture that formed did not extend to the surface of the grain, but only far enough to provide sufficient expansion to preclude further propagation.

As is common in the decrepitation of inclusions, both in nature and in the laboratory, the cracks that form from the decrepitation are seldom visible optically, however, inclusions that we measured appear not to have partially decrepitated. This conclusion is based on their appearance and on the occurrence of CO_2 inclusions of similar density in different parts (core vs. edge) of a given crystal, and in minerals of different strength in the same nodule. Most large inclusions (>100 μm) apparently decrepitated completely during the ascent of the host mineral and are now empty. Decrepitated inclusions >20 μm in diameter appear dark, seemingly opaque, from total reflection. Such decrepitation is seemingly universal in the biotite of the cumulate nodules and the phlogopite of the "skarn" nodules. We found no CO_2 (vapor or liquid) in these micas, only empty cavities.

Decrepitation is also a function of inclusion size; smaller inclusions can withstand much higher pressures (Roedder, 1965). Hence our inclusion population is biased toward the small sizes ($< \sim 100$ μm). However, inclusions $< \sim 4$ μm were usually too small for the recognition of the presence of CO_2 liquid and vapor. Decrepitated inclusions are very abundant in the pyroxenes of nodule N1 but the inclusions (now decrepitated) are large $> \sim 100$ μm; small inclusions are very rare. This may represent a bias in the initial size distribution of the inclusions rather than a greater depth of trapping.

Mechanisms of trapping. Inclusions are usually trapped in crystals growing from a melt (magma) by various processes that cause irregularity in growth conditions. Numerous mechanisms are responsible for the growth irregularities, e.g., skeletal crystal growth, but seldom can we discern what the trapping mechanism was because now we observe the completed process. However, for some of the inclusions we studied a probable trapping mechanism can be deduced.

The silicate melt inclusion shown in Fig. 5 apparently was trapped as the result of the irregularity caused by the mica on a growing surface of the pyroxene. Silicate melt adhered to the mica and was subsequently surrounded by pyroxene. The mica is not a daughter crystal although a

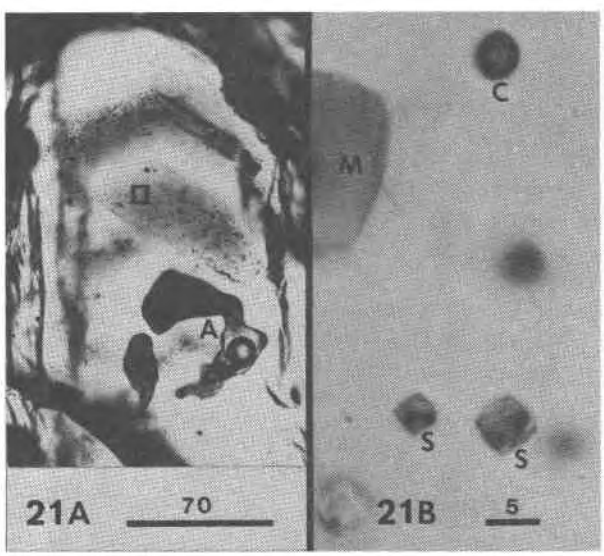

Fig. 21. (A) is a subhedral pyroxene crystal in nodule N42. Common in pyroxenes from cumulate nodules are large ameboid (A) silicate melt inclusions in the crystal core. Oscillatory zoning can be seen in the upper half of the crystal above the ameboid silicate-melt inclusion. (B) is an enlargement of the rectangular area (Fig. 21A) in the first darker, inclusion-rich band. Three types of primary inclusions are common, mica (M), silicate melt (S), and CO_2 (C). A movable meniscus can be discerned in the CO_2 inclusion but the optics are too poor to determine the homogenization temperature.

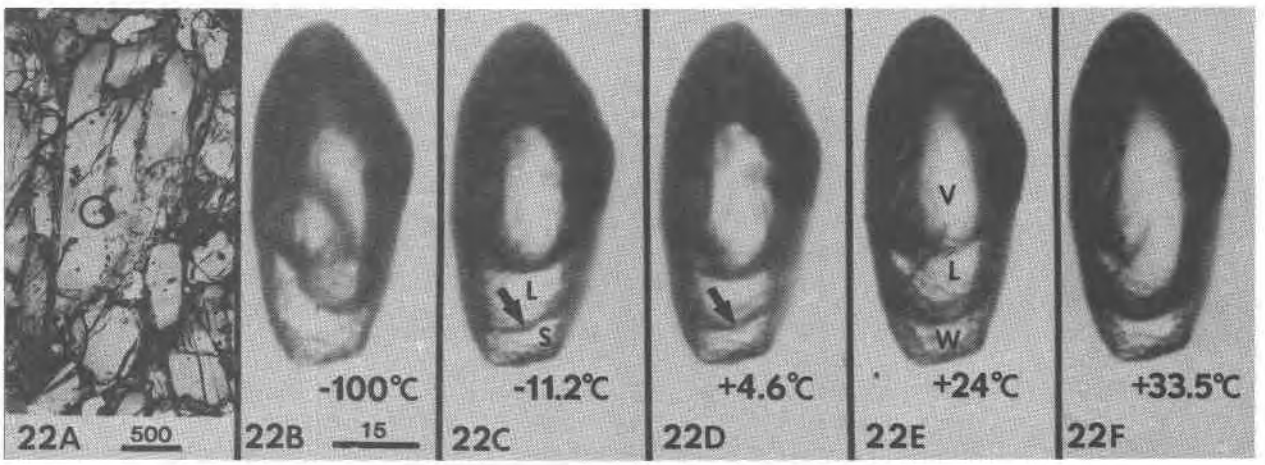

Fig. 22. (A) is a typical euhedral pyroxene crystal in nodule N81. The circle outlines a primary $CO_2 + H_2O$ inclusion. (B) shows this inclusion completely frozen at $-100°C$. Upon warming to $-11.2°C$ the CO_2 has melted ($-57.4°C$). (C) shows the somewhat jagged phase boundary that separates liquid CO_2 (L) from the solid CO_2-clathrate (S). This jagged boundary is still visible at $+4.6°C$ (D) and the CO_2 clathrate melts sluggishly at $+6.5°C$. (E) shows the three-phase inclusion CO_2 vapor (V) and CO_2 liquid (L) and liquid water (W). The CO_2 homogenizes at $+30.8°C$ in the vapor phase. (F) shows the two-phase inclusion at $+33.5°C$.

small amount of mica probably has precipitated on it from the trapped melt. This type of inclusion is common in pyroxenes from cumulate nodules. Often many mica crystals with their adhered melt will be aligned parallel to a planar growth face (often outlined by zoning). This resembles the condition of daughter crystals growing epitaxially with respect to their host (Roedder, 1979); however, these are not daughter crystals. Furthermore, homogenization of this system, mica plus melt, would give erroneous results.

Almost all of the pyroxenes in the cumulate nodules are zoned. Simple and very complex oscillatory zoning is typical; sector zoning was not observed. Most typical is a lighter-colored, uncorroded or unresorbed core, that may contain large ameboid silicate melt inclusion(s) (Fig. 21A), followed by oscillatory zoning with the darker colored banding usually containing very small inclusions. Three types (Fig. 21B) of primary inclusions are usually found (1) solid crystals, usually mica or apatite, (2) CO_2 inclusions and (3) silicate-melt inclusions. Thompson (1972) described similar zoned pyroxenes from a Vesuvian lava. His detailed microprobe analyses showed that Fe, Ti, Al are enriched in the darker zones whereas Si, Mg, are enriched in the lighter zones. Thompson noted that individual pyroxene phenocrysts had a wide range of Al_2O_3, extending from 1.0 to 9.5 wt.%. He suggested that since the $R^{2+}Al(AlSi)O_6$ pyroxene component has a marked tendency to crystallize metastably at 1 atm in the system diopside–anorthite–silica it seemed reasonable to assume that the zoning and variability of Al_2O_3 content is the result of rapid crystallization. Such crystallization, from highly supersaturated melts, usually forms skeletal growth and would be likely to trap the fluid and solid inclusions that are commonly observed in the zoned pyroxenes.

The cores of spinels (Fig. 17) in the "skarn" nodules and the cores of apatites (Fig. 13) in the cumulate nodules usually show a high density of primary solid and fluid inclusions. This is probably due to skeletal growth during the initial stages of crystal growth.

Figure 11 shows a CO_2 inclusion that formed because of an irregularity caused by a mica crystal adhering to the growing surface of a pyroxene crystal. In this case the CO_2 globule apparently preferentially wetted mica relative to pyroxene.

Solid inclusions of mica are very common in the cumulate nodule pyroxenes. The included micas (Fig. 7) usually have a hexagonal outline and commonly have a "dark" spot, usually on only one side. In rare cases (Fig. 8) the "dark" spot can be resolved as a CO_2 inclusion showing a vapor–liquid meniscus. Because the CO_2 inclusion almost always seems to occur on only one side it is reasonable to assume that the mica adhered to the growing pyroxene surface first then a globule of CO_2 "stuck" to the mica crystal. Silicate melt inclusions are also commonly found "stuck" to micas.

$CO_2 + H_2O$ inclusions. Three primary $CO_2 + H_2O$ inclusions were found in three pyroxene grains from sample N81. The water, a polar compound, always preferentially adhered to the mineral and glass walls at the positions of greatest curvature. In all three inclusions the CO_2 was ~ 60 mole% (~ 90 vol.%). The H_2O (Fig. 22A,B,C,D,E,F) was recognized by the formation of a CO_2-clathrate compound that persists above 0.0°C. The CO_2-clathrate melted at about $+7.0°C$, but this temperature was difficult to determine because of the small size of the inclusions. We assume the CO_2-clathrate compound to be $CO_2 \cdot 5\ 3/4\ H_2O$ similar to that described by Roedder (1963). No obvious melting was observed from $-56.6°C$ (CO_2 triple point melting) to the melting of CO_2-clathrate.

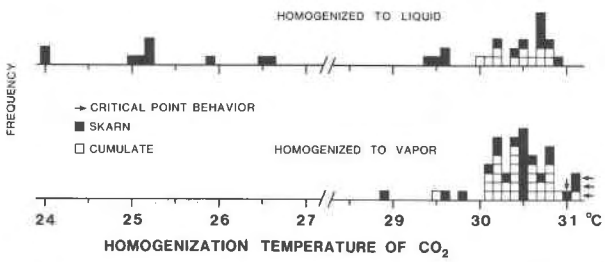

Fig. 23. Histogram plot of homogenization temperature (°C) of CO_2 for 41 inclusions from cumulate nodules (open squares) and 46 inclusions from "skarn" nodules (solid squares). The upper plot for inclusions that homogenized to liquid and the lower plot for inclusions that homogenized to vapor. Four inclusions exhibiting critical point behavior (arrow) were arbitrarily placed on the lower plot.

The $CO_2 + H_2O$ inclusions were found late in this study. Because of the possible implications of a free H_2O fluid in the melt, all the inclusions were re-examined for the possible presence of H_2O. No other $H_2O + CO_2$ inclusions were found. However, it is important to point out that the optical resolution is usually poor on small inclusions so a small amount of H_2O, especially a thin film wetting and separating the silicate glass and CO_2 fluid, could very well be missed.

The *T*h of the vapor and liquid CO_2 part of the $H_2O + CO_2$ inclusions was determined and is reported below. H_2O has essentially zero solubility in CO_2 near room temperature (Roedder, 1965), hence would not affect the CO_2 vapor–liquid homogenization temperature.

Results

CO_2 inclusions

The temperature of homogenization (*T*h) of the CO_2 was determined for 87 inclusions (Fig. 23; Table 2[2]). *T*h of pure CO_2 inclusions provides information on the density of the inclusion fluid. Figure 24 shows the density vs. temperature diagram for pure CO_2. The density of CO_2 in all nodules ranged from 0.31 to 0.72 g/cm^3.

Homogenization may occur in the liquid phase (by elimination of the bubble), in the vapor phase (by evaporation of liquid), or at the critical point (by a gradual fading of the meniscus). However, because the two-phase curve is relatively flat near the critical temperature of +31.1°C, there is a range of densities that will seem to exhibit critical behavior. All the measured inclusions were 2-phase at room temperature ($\sim 22° \pm 1$°C).

The CO_2 densities, based on measured *T*h (Fig. 23), are shown in Figure 25. CO_2 inclusions from nodules N1, N34, N42, N81, and N67 are clustered relatively tightly and have an average density of ~ 0.35 g/cm^3. Nodule N48 has 4 inclusions with an average density of ~ 0.37 g/cm^3 plus one at the critical point. Nodule N62 has 5 inclusions clustered at an average density of ~ 0.57 g/cm^3. CO_2 inclusions in three nodules, N13, N45, and N30, have a wide range of CO_2 density (0.31 to 0.72 g/cm^3) and show a bimodal density distribution on either side of the critical point density, although the bimodal distribution is somewhat accentuated by the shape of the two-phase CO_2 field.

Only three inclusions were successfully crushed in an alkaline $BaCl_2$ solution (10 g $BaCl_2$, 100 ml. H_2O, one drop NH_4OH). The bubbles expanded then immediately shrank within ~ 3 seconds to a very small size and disappeared. A white precipitate was noticed that is presumed to be insoluble $BaCO_3$ formed from the liberated CO_2.

The triple point for pure CO_2 is −56.6°C. Nine inclusions were large enough to measure the triple point (i.e., the melting temperature of the solid CO_2 with a gas phase present). The temperatures varied from −56.0 to −57.2°C. The uncertainty in these temperature measurements is high (± 1.0°C). The solid CO_2 in any particular inclusion melted essentially instantly; not within a temperature interval. Therefore, we assume the CO_2 is essentially pure CO_2.

Silicate-melt inclusions

Forty primary silicate-melt inclusions were homogenized; 23 from cumulate nodules and 17 from "skarn" nodules. This preliminary work indicates an average *T*h of 1200 ± 50°C in cumulate nodules and 1000 ± 50°C in "skarn" nodules. All silicate-melt inclusions run from cumulate nodules quench (*T*h to <500°C in ~ 2 minutes) to a clear glass, but those in the "skarn" nodules exhibit two kinds of behavior. Some inclusions (Fig. 20B) quench to a clear glass similar to those in cumulate nodules, whereas others (Fig. 20A) crystallize on quench. After quenching, those that crystallize typically have an angular bubble (Fig. 20A) and are weakly birefrigent. We have not yet made quench-furnace runs to try to reduce the uncertainties inherent in determination of melt-inclusion homogenization by means of a heating stage (e.g., slow diffusion in the melt and high gradients in the stage). Nevertheless, we believe that ~ 1200°C for cumulate and ~ 1000°C for "skarn" nodules are good estimates of the trapping temperatures.

$CO_2 + H_2O$ inclusions

The *T*h of the vapor and liquid CO_2 for the three inclusions was $\sim +30.5$°C. The homogenization was in the vapor phase and hence, the density was ~ 0.36 g/cm^3. No attempt was made to homogenize the CO_2 and H_2O phases for fear of decrepitation from high internal pressure. However, extrapolating the isochores of Swanenberg (1980; his Figures 24–27) to 1200°C yields a trapping pressure of ~ 1500 bars. This is in good agreement with pressure estimates from other inclusions in nodule N81.

[2] Table 2 contains a detailed description of the 87 inclusions; size, Th, host, density, trapping pressure and trapping depth. To receive a copy of Table 2, order Document AM-85-264 from the Business Office, Mineralogical Society of America, 2000 Florida Avenue, N.W., Washington, D.C. 20009. Please remit $5.00 in advance for the microfiche.

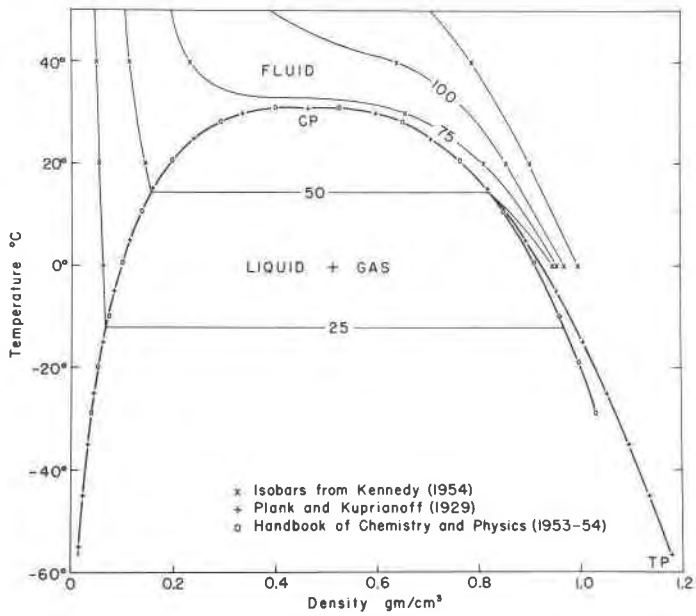

Fig. 24. Temperature–density diagram of the two-phase field in the pure system CO_2. Isobars (x) from Kennedy (1954); (+) from Plank and Kuprianoff (1929); and (o) from Hodgman (1954). (From Roedder, 1965)

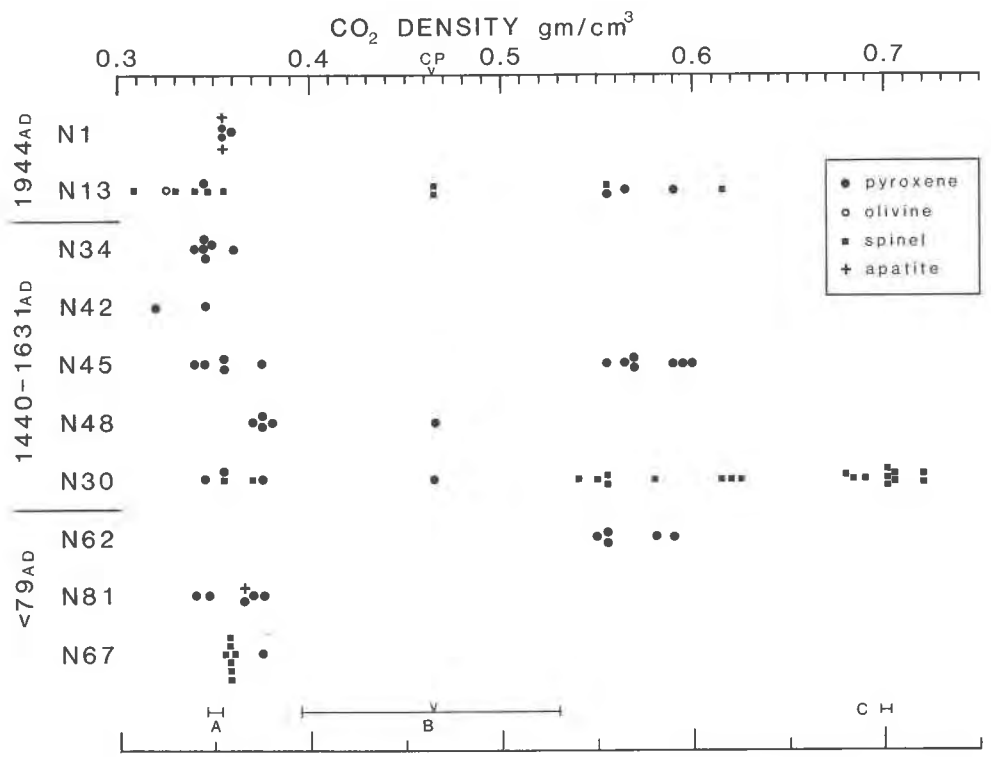

Fig. 25. Plot of CO_2 density (gm/cm^3) determined from the homogenization temperature and the homogenization behavior. The host minerals are indicated with different symbols and the nodules are grouped in the three eruptive episodes. N1, N34, N42, N45, N48, N62 and N81 are cumulate nodules and N13, N30 and N67 are "skarn" nodules. The density error bars A,B,C show the density error due to an estimated Th uncertainty of ± 0.1°C. The caret near the *B* is the position of the critical point.

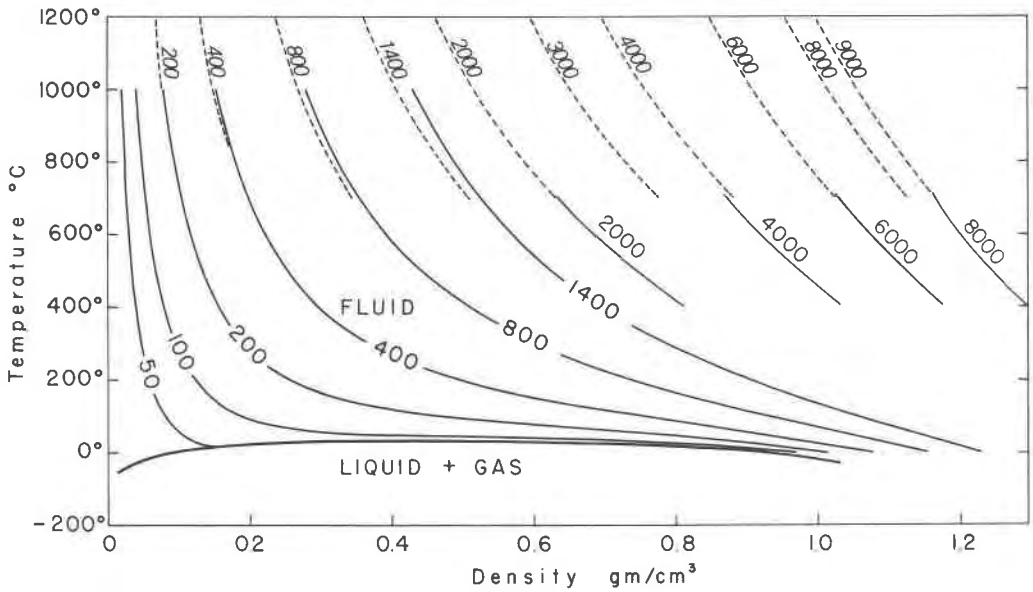

Fig. 26. Temperature-density diagram for the pure system CO_2. Solid-line isobars ≤ 1400 bar (140 MPa) from Kennedy (1954) and Roedder (1965); solid-line isobars ≥ 2000 bar (200 MPa) from the experimental data Shmonov and Shmulovich (1974) and the dashed-line isobars from a modified Redlich-Kwong equation of Kerrick and Jacobs (1981).

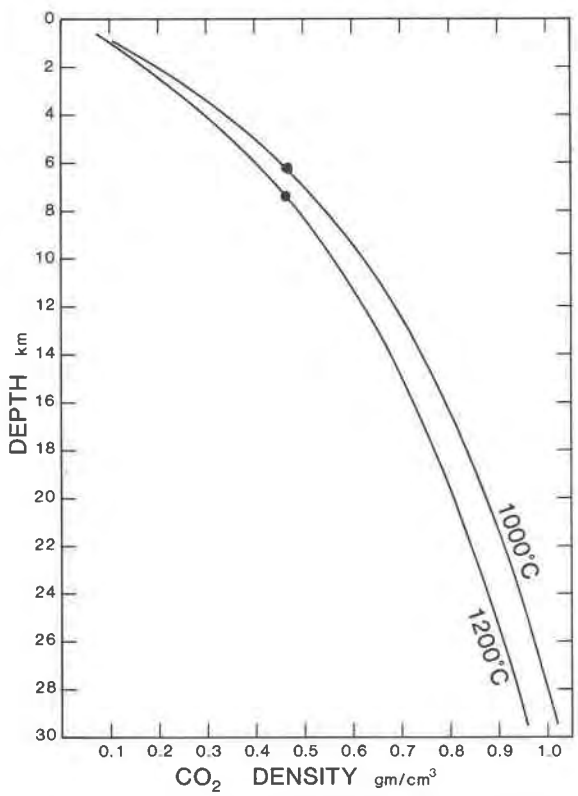

Fig. 27. Plot of CO_2 density (determined by Th of CO_2) vs depth of trapping for inclusions trapped at 1000° and 1200°C. We assume that the inclusions are 1) pure CO_2, and 2) the pressure was that of a hydrostatic head of magma with $\rho = 2.7$ gm $\cdot$ cm^{-3}. The dot on the curves marks the CO_2 critical density.

Discussion

Estimate of trapping pressure

Fluid inclusion study can usually provide the temperature of trapping or the pressure of trapping, but seldom both. Normally, the homogenization temperature is used to determine the isochore on an appropriate *P–T* diagram (Roedder and Bodnar, 1980). The pressure is usually determined by some independent method, and then the true temperature of trapping is obtained from the intersection of this pressure and the isochore. However, the presence of coeval CO_2 and silicate melt inclusions allows us to determine both the temperature and the pressure at the time of inclusion trapping. The density of the CO_2 originally filling the inclusion provides the isochore, and the silicate-melt inclusions provide the temperature ($\sim$1000 or $\sim$1200°C); the pressure is established by the intersection of temperature and isochore.

Figure 26 shows the available *P–V–T* data, both experimental and calculated, for CO_2. At high temperatures and low density the density of supercritical CO_2 is pressure dependent but relatively insensitive to temperature. The isobars (dashed lines) calculated by Kerrick and Jacobs (1981) were used at 1000°C for "skarn" and 1200°C for cumulate nodules. All the inclusions appear to have crystallized in the range $\sim$925 to $\sim$3550 bars. No special relationship was seen between the pressures determined for the two types of nodules or for the three eruptive episodes.

Limitations of the present study

A series of factors limit the accuracy of the pressure determinations. First, the technique for determination of

Th CO_2 resulted in a temperature uncertainty of ± 0.1°C. Because of the very flat top of the two-phase CO_2 curve (Fig. 24) the corresponding uncertainty in the CO_2 density varies. The lengths of the bars labelled A,B,C in Fig. 25 show what the density uncertainty would be with a temperature uncertainty of ± 0.1°C. On the low- and high-density sides (A + C) the density uncertainty is approximately ± 0.005 g/cm^3. At the critical point the density uncertainty is approximately ± 0.08 g/cm^3 (B). However, because homogenization is to liquid on one side and to vapor on the other side of the critical point and this difference is easily recognized, the uncertainty is $\sim 50\%$ less $= \pm 0.04$ g/cm^3.

Second, we have assumed a trapping temperature of 1000 and 1200°C for the "skarn" and cumulate nodules, respectively. The value for the cumulate nodules (1200°C) is in the range suggested by Dolfi and Trigila (1978) for the 1944 lavas and by Baldridge et al. (1981) for other similar leucite-basanite lavas. At a CO_2 inclusion density of 0.7 g/cm^3, a trapping temperature uncertainty of ± 50°C (in the range 1000 to 1200°C) yields a pressure uncertainty of ± 200 bars or $\sim \pm 0.8$ km (magma column $\rho = 2.7$ g/cm^3). At a CO_2 inclusion density of 0.35 g/cm^3, a trapping temperature uncertainty of ± 50°C (in the range 1000° to 1200°C) yields a pressure uncertainty of ± 50 bars or $\sim \pm 0.2$ km (magma column $\rho = 2.7$ g/cm^3).

Third, the lack of appropriate experimental P–V–T data for CO_2 makes extrapolation or calculation to higher temperatures uncertain. We have used the isobars calculated by Kerrick and Jacobs (1981) at a temperature of 1000 and 1200°C. Figure 26 shows the lack of agreement between the experimental values and the calculated values especially at higher pressures. This points up the need for adequate CO_2 P–V–T data at high temperatures and pressures.

Fourth, we assume that volume of the CO_2 inclusions we studied has not changed significantly during their ascent. All CO_2 inclusions were the result of simultaneous trapping of supercritical CO_2 and a small amount of melt (~ 1 to ~ 10 vol.%) in a host mineral at ambient conditions. At room temperature and pressure the cavity volume has theoretically changed by (1) shrinkage and crystallization on the walls by the melt, (2) expansion of the host mineral from pressure reduction, (3) shrinkage of the host minerals from cooling, and (4) expansion by pressure of the trapped CO_2 on the inclusion walls. We judge that the resultant effect from the above factors is well below errors from other sources and can generally be ignored at this time. Although decrepitation was common in some nodules, we believe that none of the CO_2 inclusions we measured have partially decrepitated and lost CO_2. However, because larger CO_2 inclusions had decrepitated, and denser CO_2 inclusions would decrepitate more easily, our sample was biased in CO_2-inclusion size and perhaps in density.

Fifth, Kirby and Green (1980) have suggested that olivine can easily deform plastically during eruption, leading to incorrect densities and hence pressures, and transmission electron micrographs of some minute inclusions in olivine show dislocation loops indicating expansion. However, the petrographic evidence on the much larger inclusions reported here suggests no recognizable expansion. Much more extensive TEM studies are in order.

In spite of these assumptions and shortcomings we believe that our preliminary study can place some constraints on nodule petrogenesis.

Depth, conditions and environment of crystallization

If we assume that the inclusions were trapped in a pressure regime resulting solely from the hydrostatic pressure of the magma column ($\rho = 2.7$ g/cm^3) then we can relate the density of the CO_2 inclusion (from the *Th* determination) and depth (Fig. 27) for any particular trapping temperature. However, if some of the nodules crystallized in an isolated environment surrounded by country rock (sealed pockets), then the pressure might have been equal to the lithostatic load. Nunziata and Rapolla (1981) have estimated the density of the basement rock (carbonates) in the Naples area to be 2.7 g/cm^3. Thus any lithostatic pressure effects would be similar to the hydrostatic pressure of the magma column. For all CO_2 inclusions the crystallization depth ranges from ~ 3.5 to ~ 13 km. The greater the density of the magma column, the shallower the inclusion trapping would be at constant density. A magma column density difference of 0.1 g/cm^3 would be equivalent to a $\sim 4\%$ change in depth.

Zoning is very abundant in the clinopyroxenes in the seven cumulate nodules. Simple and complex oscillatory zoning are most common. Thompson (1972) reports zoning in augite phenocrysts from Vesuvius lavas. He describes the typical zoned crystal as consisting of a very irregular, colorless corroded core mantled by pale and dark oscillatory and sector banding. Barton et al. (1982) report complex zoning of clinopyroxenes from the lavas of Vulsini, Italy. Corroded pyroxene cores that are mantled by later oscillatory growth are interpreted as evidence for magma mixing.

Although many origins have been proposed for oscillatory zoning, rapid changes in temperature, pressure, $f(H_2O)$, $f(CO_2)$ and/or $f(O_2)$ are most commonly invoked. The rapid fluctuations necessary to produce the oscillatory zoning that we observe suggests a shallow crustal environment. Fluctuations in total pressure, for example, from various volcanic processes, would be propagated through a shallow magma body rapidly whereas deeper in the crust these changes would probably be damped.

The range of densities (Fig. 25) in nodules N13, N45, and N30 is enigmatic. This CO_2 inclusion density range exists among crystals separated by only millimeters in the same thick section; and within certain spinel crystals in nodules N13 and N30, a similar density range exists within tens of micrometers with denser inclusions in the interior of the crystal. A possible scenario is offered and discussed below; however, it is not adequate to explain all the data. The authors would gladly entertain plausible suggestions.

The possibility is that as the magma ascended, growing phenocrysts would trap supercritical CO_2 globules at different depths and hence would result in inclusions with different densities. This process would be nearly isothermal.

Rock has a very low thermal conductivity, thus an ascending magma would not cool significantly. This situation seems reasonable for the pyroxenes—a common lava phenocryst—in nodule N45. However, CO_2 inclusions have not been reported in the phenocryst pyroxenes from any of these lavas. Furthermore, nodule N45 contains ~25% biotite—a rare phenocryst phase. It appears unlikely that the pyroxene crystals in nodule N45 are normal phenocrysts produced in the bulk of the magma. Hercynitic, low Cr-spinels, abundant in the "skarn" nodules, are not reported as phenocrysts in the lavas and tephra. In light of the unusual mineralogy of the "skarn" nodules it seems unlikely that these represent phases crystallizing from the main bulk of the ascending magma.

Cumulate nodules. All the mineral phases in the seven cumulate nodules have crystallized from a silicate melt in the presence of a coexisting, immiscible and supercritical CO_2 fluid. Our preliminary data cannot resolve any differences among the cumulate nodules from the three eruptive episodes. The cumulate textures and preferred mineral orientation observed in the nodules are compatible with crystal settling during part of their formation. The bent micas and interstitial glass suggest that they were ejected while a crystal mush.

The melts that were trapped and from which the host minerals crystallized were saturated with respect to CO_2 and in one case a mixture of CO_2 and H_2O. Although these inclusions are common in some crystals, the CO_2 inclusions give us no information on the amount of CO_2 in the magma. The variability in abundance of the CO_2 inclusions is merely a consequence of the accidental nature of the trapping process. Furthermore we cannot say anything about the CO_2 content of the common lavas and tephra erupted from Vesuvius. Roedder (1965) examined one sample each of Vesuvius 1944 and 1858 lavas and did not find any CO_2 inclusions. This suggests that the melts from which the nodules formed were not strictly identical to the bulk of the magma ejected as lava or tephra. Perhaps these melts have been modified by processes such as fractionation and/or contamination.

"Skarn" nodules. Hermes and Cornell (1978) defined the "skarn" nodules on the basis of their unusual mineralogy and major-element chemistry. They invoked metasomatic processes to transform the country rock (carbonate) to a "skarn" assemblage. The term "skarn" as originally defined by Törnebohm (1875) is a rock that was transformed by essentially solid-state reaction processes. We find primary silicate melt and CO_2 inclusions in all the "skarn" nodule phases, indicating crystallization of these nodules in the presence of, and hence presumably from, a melt. Furthermore, the range of densities in the CO_2 inclusions in the "skarn" nodules and the apparent two types of silicate-melt inclusions indicate that their crystallization history was complex. Perhaps the unusual rock compositions may be adequately explained by the formation of a contaminated magma in a zone of lava-country rock assimilation. Varekamp (1979, 1983) ascribes the origin of "skarn" nodules from the Vulsinian volcanic area to fragments of a contaminated zone in a shallow magma chamber. The occurrence of nodules being ejected at the end of the eruptive episodes (at least for the 1944 eruption) is consistent with their postulated formation around the periphery of the magma chamber. After lava eruptions empty most of the chamber, late-stage phreato-magmatic events may excavate pieces (nodules) of this zone, together with the ejection of the typical late-stage, fine-grained pyroclastics.

Knowledge of the volatile content (CO_2 and H_2O) of the glasses trapped as silicate melt inclusions or as interstitial material would bear greatly on the various theories of nodule origin. Harris (1981) has developed a method of gas analysis that would be ideally suited for such a study.

Origin of CO_2

Although we do not have any data that might reveal the origin of the supercritical CO_2 fluid, one (or a combination) of three possible sources might have been involved: (1) original mantle CO_2; (2) deep assimilation of sinking major crustal carbonate blocks or carbonate-rich sediments; (3) local shallow carbonate assimilation in the volcanic edifice. Oxygen isotope data may be of little use to recognize carbonate assimilation because CO_2 bubbling through a silicate melt at high temperatures will rapidly undergo oxygen isotopic exchange and equilibrate with the melt (Muehlenbachs and Kushiro, 1974). Carbon isotope data may be of more value. Regardless of the source of the CO_2, rapid vesiculation of the CO_2 during ascent must provide at least a part of the eruption energy. Decrepitation of CO_2 inclusions in the erupting minerals would add to this gas release.

Conclusions

1. All the minerals in the ten nodules we studied have crystallized in the presence of and hence presumably from a silicate melt.

2. An immiscible supercritical CO_2 fluid was also present at the time of crystallization of all ten nodules. Water was present in the CO_2 fluid in three inclusions from nodule N81.

3. Seven cumulate nodules have a magmatic origin and some have textures that suggest crystal setting and fractionation processes.

4. The three "skarn" nodules studied are also magmatic products and probably represent the crystallization of contaminated magma from a peripheral assimilation zone of lava plus carbonate country rock. The two types of silicate-melt inclusions suggest that at least locally, different melt compositions were present.

5. Six nodules, N1, N34, N42, N48, N81, and N67 appear to have crystallized in the range of ~4 to ~7 km. Nodule N62 appears to have crystallized at ~10 km.

6. Three nodules, N13, N45 and N30 each contain CO_2 inclusions that have a bimodal CO_2 density distribution and appear to be trapped in the range of ~3.5 to ~13 km. The origin of the range of densities within a single thick section or within a single crystal has yet to be adequately explained.

7. The homogenization temperatures of silicate-melt inclusions indicate a temperature of ~1200°C during cumulate nodule crystallization and ~1000°C during "skarn" nodule crystallization.

8. A major zone of crystallization of the cumulate and "skarn" nodules from the 3 non-Plinian eruptions seems to have been within the underlying carbonate country rocks at a depth of from ~3.5 to ~13.0 km. This depth range may also contain the magma reservoir(s) for the lava erupted during these episodes.

Acknowledgments

This study was undertaken during a research fellowship at the U.S. Geological Survey, Reston granted to B. De Vivo by the National Research Council of Italy (CNR). Dr. H. T. Haselton, Jr. (USGS) kindly assisted with the *P–V–T* calculations based on the equations of Kerrick and Jacobs (1981). The careful reviews of R. I. Tilling (USGS), D. E. Voigt (USGS), R. J. Arculus (University of Michigan) and M. L. Crawford (Bryn Mawr) are gratefully acknowledged.

References

Alfano, G. B. and Friedlander, I. (1929) Die Geschichte des Vesuv: Ulm, a.D., K. Hohn.

Arculus, R. J. and Wills, K. J. A. (1980) The petrology of plutonic blocks and inclusions from the Lesser Antilles island arc. Journal of Petrology, 21, 743–799.

Baldridge, S. W., Carmichael, I. S. E., and Albee, A. L. (1981) Crystallization paths of leucite-bearing lavas: Examples from Italy. Contributions to Mineralogy and Petrology, 76, 321–335.

Barberi, F., Bizouard, H., Clocchiatti, R., Metrich, N., Santacroce, R., and Sbrana, A. (1981) The Somma-Vesuvius magma chamber: a petrological and volcanological approach. Bulletin Volcanologique, 44, 295–315.

Barberi, F. and Leoni, L. (1980) Metamorphic carbonate ejecta from Vesuvius Plinian eruptions: Evidence of the occurrence of shallow magma chambers. Bulletin Volcanologique, 43, 107–120.

Barton, M., Varekamp, J. C., and Van Bergen, M. J. (1982) Complex zoning of clinopyoxenes in the lavas of Vulsini, Latium, Italy: Evidence for magma mixing. Journal of Volcanology and Geothermal Research, 14, 361–388.

Bonasia, V., Del Pezzo, E., Pingue, F., Scandone, R., and Scarpa, R., (1983) Eruptive history, seismic and ground deformation activity at Mt. Vesuvius, Italy: International Association of Volcanology and Chemistry of the Earth's Interior, Programme and Abstracts. International Union of Geodesy and Geophysics 18th General Assembly, 29.

Cortini, M. and Hermes, O. D. (1981) Sr isotope evidence for a multi-source origin of the potassic magmas in the Neapolitan area (S. Italy). Contributions to Mineralogy and Petrology, 77, 47–55.

Cortini, M. and Scandone, R. (1982) The feeding system of Vesuvius between 1754 and 1944: Journal of Volcanology and Geothermal Research, 12, 393–400.

Cundari, A. (1982) Petrology of clinopyroxenite ejecta from Somma-Vesuvius and their implications. Tschermak's mineralogische und petrographische Mitteilungen, 30, 17–35.

Cunningham, C. G. and Corollo, C. (1980) Modification of a fluid-inclusion heating/freezing stage. Economic Geology, 75, 335–337.

Delibrias, G., Di Paola, G. M., Rosi, M., and Santacroce, R. (1979) La storia eruttiva del complesso vulcanico Somma Vesuvio ricostruita dalle successioni piroclastiche del Monte Somma. Rendiconti della Societa Italiana di Mineralogia e Petrologia, 35, 411–438.

Dolfi, D. and Trigila, R. (1978) The role of water in the 1944 Vesuvius eruption. Contributions to Mineralogy and Petrology, 67, 297–304.

Gasparini, C., Iannaccone, G., Scandone, P. and Scarpa, R. (1982) Seismotectonics of the Calabrian arc. Tectonophysics, 84, 267–286.

Giannetti, B. (1982) Cumulate inclusions from K-rich magmas, Roccamonfina volcano, Italy. Earth and Planetary Science Letters, 57, 313–335.

Harris, D. M. (1981) The microdetermination of H_2O, CO_2, and SO_2 in glass using a 1280°C microscope vacuum heating stage, cryopumping, and vapor pressure measurements from 77 to 273 K. Geochimica et Cosmochimica Acta, 45, 2023–2036.

Hawkesworth, C. J. and Vollmer, R. (1979) Crustal contamination versus enriched mantle: $^{143}Nd/^{144}Nd$ and $^{87}Sr/^{86}Sr$ evidence from the Italian volcanics. Contributions to Mineralogy and Petrology, 69, 151–165.

Hermes, O. D. and Cornell, W. C. (1978) Petrochemical significance of xenolithic nodules associated with potash-rich lavas of Somma-Vesuvius volcano. NSF final technical report, University of Rhode Island.

Hermes, O. D. and Cornell, W. C. (1981) Quenched crystal mush and associated magma compositions as indicated by intercumulus glasses from Mt. Vesuvius, Italy. Journal of Volcanology and Geothermal Research, 9, 133–149.

Hermes, O. D. and Cornell, W. C. (1983) The significance of mafic nodules in the ultra-potassic rocks from Central Italy—reply. Journal of Volcanology and Geothermal Research, 16, 166–172.

Hodgman, C. D. (1954) Handbook of Chemistry and Physics, 35th ed: Chemical Rubber Publishing Co., Cleveland, Ohio, 3163 p.

Hollister, L. S. and Crawford, M. L. (1981) Short course in fluid inclusions: Applications to petrology. Mineralogical Association of Canada, Calgary.

Imbo, G. (1950) Successione e spessori delle formazioni geologiche nel basamento del Somma-Vesuvio. Annali dell'Osservatorio Vesuviano 5th Ser. 1–15.

Ippolito, F., D'Argenio, B., Pescatore, T., and Scandone, P. (1975) Structural-stratigraphic units and tectonic framework of southern Apennines. In C. H. Squyres, Ed., Geology of Italy, 2, p. 317–328. The Earth Sciences Society of the Libyan Arab Republic, Tripoli.

Kennedy, G. C. (1954) Pressure-volume relations in CO_2 at elevated temperatures and pressures. American Journal of Science, 252, 225–241.

Kerrick, D. M. and Jacobs, G. K. (1981) A modified Redlich–Kwong equation for H_2O, CO_2, and H_2O–CO_2 mixtures at elevated pressures and temperatures. American Journal of Science, 281, 735–767.

Kirby, S. H. and Green, H. W., II (1980) Dunite xenoliths from Hualalai volcano: Evidence for mantle diapiric flow beneath the island of Hawaii. American Journal of Science, 280-A, 550–575.

Muehlenbachs, K. and Kushiro, I. (1974) Oxygen isotope exchange and equilibrium of silicates with CO_2 and O_2. Carnegie Institution of Washington Yearbook, 73, 232–236.

Ninkovich, D. and Hays, J. D. (1972) Mediterranean island arcs and origin of high potash volcanoes. Earth and Planetary Science Letters, 16. 331–345.

Nunziata, C. and Rapolla, A. (1981) Interpretation of gravity and magnetic data in the Phlegraean fields geothermal area, Naples,

Italy. Journal of Volcanology and Geothermal Research, 9, 209–225.

Plank, R. and Kuprianoff, J. (1929) Thermal qualities of carbon dioxide in gaseous, liquid, and solid state. Zeitschrift für Technische Physik, *10*, 93–101; (see also Zeitschrift für die Gesamte Kaelte-Industrie, Beihefte, 1 (1929), 1).

Poty, B., Leroy, J., and Jachimowicz, L. (1976) Un nouvel appareil pour la mesure des temperatures sous le microscope: l'installation de microthermometrie Chaixmeca. Bulletin Minéralogie, 99, 182–186 (in French; translated in Fluid Inclusion Research—Proc. COFFI 1976, 9, 173–178.

Rittmann, A. (1933) Die geologisch bedingte Evolution und Differentiation des Somma-Vesu-Magmas. Zeitschrift für Vulkanologie, 15, 8–94.

Roedder, E. (1963) Studies of Fluid inclusions II: Freezing data and their interpretation. Economic Geology, 58, 167–211.

Roedder, E. (1965) Liquid CO_2 inclusions in olivine-bearing nodules and phenocrysts from basalts. American Mineralogist, 50, 1746–1782.

Roedder, E. (1970) Application of an improved crushing microscope stage to studies of the gases in fluid inclusions. Schweizerische Mineralogische und Petrographische Mitteilungen, 50, 41–58.

Roedder, E. (1976) Fluid-inclusion evidence on the genesis of ores in sedimentary and volcanic rocks. In K. H. Wolf, Ed., Handbook of Strata-Bound and Stratiform Ore Deposits, 2, p. 67–110. Elsevier, Amsterdam.

Roedder, E. (1979) Origin and significance of magmatic inclusions. Bulletin Minéralogie, 102, 487–510.

Roedder E. and Bodnar, R. J. (1980) Geologic pressure determinations from fluid inclusion studies. Annual Review of Earth and Planetary Science, 8. 263–301.

Rosi, M., Sbrana, A. and Principe, C. (1983) The Phlegraean Fields: Structural evolution, volcanic history and eruptive mechanisms. Journal of Volcanology and Geothermal Research, 17, 273–288.

Santacroce, R. (1983) A general model for the behavior of the Somma-Vesuvius volcanic complex. Journal of Volcanology and Geothermal Research, 17, 237–248.

Savelli, C. (1967) The problem of rock assimilation by Somma-Vesuvius magma: I. Composition of Somma and Vesuvius lavas. Contributions to Mineralogy and Petrology, 16, 328–353.

Savelli, C. (1968) The problem of rock assimilation by Somma-Vesuvius magma: II. Composition of sedimentary rocks and carbonate ejecta from the Vesuvius area. Contributions to Mineralogy and Petrology, 18, 43–64.

Sheridan, M. F., Barberi, F., Rosi, M., and Santacroce, R. (1981) A model for Plinian eruptions of Vesuvius. Nature, 289, 282–285.

Shmonov, V. M. and Shmulovich, K. I. (1974) Molal volumes and equation of state of CO_2 at temperatures from 100 to 1000°C and pressure from 2000 to 10,000 bars. Doklady Akadamy Nauk SSSR, 217, p. 935–938. (in Russian; translation in Doklady Acadamy Sciences USSR, 217 (1975) p. 206–209).

Sorby, H. C. (1858) On the microscopical structure of crystals, indicating the origin of minerals and rocks. Quarterly Journal of the Geological Society of London, 14, pt. 1, 453–500.

Swanenberg, H. E. C. (1980) Fluid inclusions in high-grade metamorphic rocks from S.W. Norway. Geologica Ultraiectina, No. 25, 1–147.

Taylor, H. P., Jr., Giannetti, B., and Turi, B. (1979) Oxygen isotope geochemistry of the potassic igneous rocks from the Roccamonfina volcano, Roman comagmatic region, Italy. Earth and Planetary Science Letters, 46, 81–106.

Thompson, R. N. (1972) Oscillatory and sector zoning in augite from a Vesuvian lava. Carnegie Institution of Washington Yearbook 71, 463–470.

Törnebohm, A. E. (1875) Geognostisk beskrifning öfver Persbergets grufvefält. Sveriges geologiska undersökning, C14, 1–21.

Turi, B. and Taylor, H. P., Jr. (1976) Oxygen isotope studies of potassic volcanic rocks of the Roman province, Central Italy. Contributions to Mineralogy and Petrology, 55, 1–31.

Varekamp, J. C. (1979) Geology and petrology of the Vulsinian volcanic area, Lazio, Italy. Ph.D. thesis, Utrecht. Geologica Ultraiectina, 22, 394 p.

Varekamp J. C. (1983) The significance of mafic nodules in the ultrapotassic rocks from central Italy-Discussion. Journal of Volcanology and Geothermal Research, 16, 161–165.

Wager, L. R., Brown, G.M., and Wadsworth, W.J. (1960) Types of igneous cumulates. Journal of Petrology, 1, 73–85.

Washington, H. S. (1906) The Roman comagmatic region. Carnegie Institute Publication no. 57.

Zambonini, F. (1936) Mineralogia Vesuviana, Torino, Rosenberg and Sellier.

Manuscript received, January 30, 1984;
accepted for publication, October 30, 1984.